Hindawi Publishing Corporation
International Journal of Photoenergy
Volume 2016, Article ID 6193502, 9 pages
http://dx.doi.org/10.1155/2016/6193502

Research Article

$ZnSnS_3$: Structure Prediction, Ferroelectricity, and Solar Cell Applications

Radi A. Jishi[1] and Marcus A. Lucas[2]

[1]*Department of Physics, California State University, Los Angeles, CA, USA*
[2]*Department of Electrical Engineering, California State University, Los Angeles, CA, USA*

Correspondence should be addressed to Radi A. Jishi; rjishi@calstatela.edu

Received 10 June 2016; Revised 3 October 2016; Accepted 18 October 2016

Academic Editor: Hongxia Wang

The rapid growth of the solar energy industry is driving a strong demand for high performance, efficient photoelectric materials. In particular, ferroelectrics composed of earth-abundant elements may be useful in solar cell applications due to their large internal polarization. Unfortunately, wide band gaps prevent many such materials from absorbing light in the visible to mid-infrared range. Here, we address the band gap issue by investigating the effects of substituting sulfur for oxygen in the perovskite structure $ZnSnO_3$. Using evolutionary methods, we identify the stable and metastable structures of $ZnSnS_3$ and compare them to those previously characterized for $ZnSnO_3$. Our results suggest that the most stable structure of $ZnSnS_3$ is the monoclinic structure, followed by the metastable ilmenite and lithium niobate structures. The latter structure is highly polarized, possessing a significantly reduced band gap of 1.28 eV. These desirable characteristics make it a prime candidate for solar cell applications.

1. Introduction

Ferroelectrics are materials that possess spontaneous electric polarization. This results from a lack of inversion symmetry; all ferroelectric crystals are noncentrosymmetric. Due to intrinsic polarization, ferroelectrics may serve as light harvesters in photovoltaic devices [1–6]. In a semiconductor p-n junction acting as a photovoltaic device, the built-in potential across the depletion layer is used to separate the photoexcited electron-hole pairs; the maximum open-circuit voltage is thus almost equal to the semiconductor band gap. In a ferroelectric, on the other hand, the separation of the photoexcited pairs is due to the built-in potential induced by the intrinsic polarization; this makes possible the realization of open-circuit voltages that far exceed the band gap [7–17].

Among the most important ferroelectrics are metal oxide perovskites with the general formula ABO_3, where A and B are metal cations (B is usually a transition metal). Well-known examples of such ferroelectrics are $BaTiO_3$ and $LiNbO_3$. These oxides have relatively large internal electric fields that could be exploited in photovoltaic applications. However, progress in this area has been hampered by the fact that these ferroelectrics have a large band gap (3-4 eV), which makes them unsuitable for efficient light harvesting. The large band gap is due to the strong ionic bonding between the transition metal B and oxygen, which, in turn, is due to the large difference in electronegativity between these atoms. In ABO_3, the highest valence band is derived from oxygen 2p orbitals, while the low conduction bands are derived from the transition metal 3d states.

To reduce the band gap in ferroelectrics, different strategies have been implemented. Choi et al. [18] alloyed the ferroelectric $Bi_4Ti_3O_{12}$, which has an optical band gap between 3.1 and 3.6 eV [19–21], with $LaCoO_3$, which is a Mott insulator with a small band gap of 0.1 eV [22]. From X-ray diffraction and scanning transmission electron microscopy, they concluded that some La atoms substitute for some Bi atoms at specific sites, and some Co atoms occupy some Ti sites. Since Co is more electronegative than Ti (1.88 versus 1.54), Co-O bond is less ionic than Ti-O bond, and a reduction in the band gap is expected. Indeed, a reduction of up to 1 eV was observed.

In another approach, Grinberg et al. [23] placed two different transition metal cations on the perovskite B-site,

with one atom driving ferroelectricity and the other producing a band gap in the visible range. They mixed the ferroelectric oxide potassium niobate ($KNbO_3$) with barium nickel niobate ($BaNi_{1/2}Nb_{1/2}O_{3-\delta}$) so as to introduce Ni^{2+} on the B-site along with an oxygen vacancy which can give rise to gap states in the host $KNbO_3$ crystal. The solid solutions thus formed, $[KNbO_3]_{1-x}[BaNi_{1/2}Nb_{1/2}O_{3-\delta}]_x$ with $x = 0.1$ to 0.5, were ferroelectric, with a direct band gap ranging from 1.1 to 3.38 eV.

In some multiferroics, which exhibit a magnetic order alongside the ferroelectric one, a somewhat smaller band gap exists. In $BiFeO_3$ the band gap is 2.7 eV [24, 25]. It is thus expected that multiferroics, such as $BiFeO_3$ and Bi_2FeCrO_6 [26, 27], would be more promising candidates for solar cell applications. In Bi_2FeCrO_6 epitaxial thin films, the optical band gap depends on the degree of Fe-Cr ordering. This dependence results from the hybridization of the 3d orbitals in Fe and Cr with the 2p orbitals in oxygen. Nechache et al. [28] investigated the effect of Fe/Cr ordering on the band gap and found that, under the right film growth conditions, the gap can be tuned all the way from 2.7 eV down to 1.5 eV.

An important class of ferroelectric oxides is those that crystallize in the $LiNbO_3$ structure (LN-structure) with space group R3c. These crystals are noncentrosymmetric, with a large polarization. LN-$ZnSnO_3$, synthesized under a pressure of 7 GPa [29], has a polarization given by 59 $\mu C/cm^2$. Other LN-type polar oxides synthesized under high pressure include $CdPbO_3$ [30], $PbNiO_3$ [30, 31], $GaFeO_3$ [32], and $LiOsO_3$ [33]. Ilmenite $ZnGeO_3$ transforms to an orthorhombic perovskite phase at 30 GPa, and upon releasing the pressure, to the LN-structure [34, 35], with a polarization of about 60 $\mu C/cm^2$ [36, 37]. Several other LN-type oxides, such as $MnTiO_3$ [38–41], $MnSnO_3$ [42, 43], $FeTiO_3$ [39, 43–45], $FeGeO_3$ [46], $MgGeO_3$ [35, 39, 47], and $CuTaO_3$ [48], were similarly obtained during decompression from the perovskite-type phase, which is stable at high pressure. More recently, LN-type $ZnTiO_3$, with a large polarization of 88 $\mu C/cm^2$, has been synthesized in this fashion [49].

Polar oxide semiconductors of the LN-type have wide band gaps. For example, $ZnSnO_3$ has a band gap of 3.3–3.7 eV [50, 51]; such values are typical for this class of materials. However, it has been noted that the band gap in $ZnSnO_3$ is very sensitive to variations in the lattice constants, and suggestions have been made to tune the band gap by growing $ZnSnO_3$ films on a substrate with some degree of lattice mismatch [52], by substituting sulfur for oxygen [53], or by substitutional doping with calcium or barium [54].

In this work, we carry out first-principles calculations, using density functional theory (DFT), on three LN-type crystals with large remnant polarization, namely, $ZnSnO_3$, $ZnGeO_3$, and $ZnTiO_3$. We show that, upon using the modified Becke-Johnson (mBJ) exchange potential [55], the correct sizes of the band gaps are calculated for these crystals. Having established the validity of this computational method in producing the correct band gaps for this family of compounds, we then focus on $ZnSnO_3$ and study the effect of substituting sulfur for oxygen. Previous work has already validated the substitution of sulfur for oxygen and vice versa as a way of tailoring band gaps in other materials [56–58]. Since the structure of the resulting compound, $ZnSnS_3$, is unknown, we carry out extensive calculations using evolutionary algorithms in order to determine its structure. We find that the most stable form of $ZnSnS_3$ has a monoclinic structure, followed closely by the ilmenite and lithium niobate (LN) forms. The monoclinic and ilmenite phases are not polar, but the LN-phase is ferroelectric, with significant polarization and a small band gap of 1.28 eV.

2. Methods

To predict the stable and metastable structures of $ZnSnS_3$, two different evolutionary methods, implemented in the codes USPEX and CALYPSO, were employed. The USPEX (Universal Structure Predictor: Evolutionary Xtallography) software [59–61], developed by Oganov, Glass, Lyakhov, and Zhu, features local optimization, real-space representation, and variation operators that mimic natural evolution. The CALYPSO (Crystal Structure Analysis by Particle Swarm Optimization) software [62], developed by Wang et al., uses local structural optimization and the particle swarm optimization (PSO) method to update structures.

The first step, in both methods, is to generate a population of random crystal structures, each with a symmetry described by a randomly chosen space group. Once a space group is selected, appropriate lattice vectors and atomic positions are generated. Each generated structure is optimized using density functional theory, and its free energy (known as the fitness function) is calculated. The structure optimization is carried out using the VASP [63–65] software, which uses a plane wave basis for expanding the electronic wave function. Each structure is optimized in four steps, beginning with a coarse optimization, followed by increasingly accurate iterations. In the last optimization step, the kinetic energy cutoff for plane wave expansion of the wave function is 600 eV. The optimized structures of the initially generated population constitute the first generation, with each member being called an individual. A new generation is then produced, with some of its members being generated randomly while others are obtained from the best structures (those with lowest energy) of the previous generation. In USPEX, new individuals (offspring) are produced from parent structures by applying variation operators such as heredity, mutation, or permutation. In the PSO method, a new structure is generated from a previous one by updating the atomic positions using an evolutionary algorithm. The structures in the new generation are optimized, and the best among them serve as precursors for structures in the next generation. The process continues until convergence to the best structures is achieved.

Band gaps, band structures, and densities of states were calculated using the all-electron, full-potential, linearized, and augmented plane wave method as implemented in the WIEN2K [66] software suite. Here, space is divided into two regions. One region comprises the interior of nonoverlapping muffin-tin spheres centered on the atomic sites, while the rest of the space (the interstitial) forms the other region. The electronic wave function is expanded in terms of a set of basis functions which take different forms in each distinct

Table 1: The predicted most stable structures of $ZnSnS_3$ at atmospheric pressure. The space groups that describe the symmetry of the structures, the lattice constants (in Å), the angles between the lattice vectors (in degrees), and the relative energies per atom (in eV) are shown. For ease of comparison, the energy per atom of the most stable structure is set equal to zero.

Space group (number)	Lattice constants (Å) and angles (degrees)	Energy/atom (eV)
$P2_1$ (4)	$a = 8.714$, $b = 6.398$, $c = 3.752$, $\alpha = \beta = 90$, $\gamma = 92.362$	0.000
R-3 (148)	$a = b = c = 7.016$, $\alpha = \beta = \gamma = 53.689$	0.040
R3c (161)	$a = b = c = 6.761$, $\alpha = \beta = \gamma = 55.799$	0.068
$P6_3$/m (176)	$a = b = 3.737$, $c = 17.405$, $\alpha = \beta = 90$, $\gamma = 120$	0.074
R32 (155)	$a = b = c = 6.828$, $\alpha = \beta = \gamma = 55.122$	0.089
$P6_3$ (173)	$a = b = 6.187$, $c = 6.431$, $\alpha = \beta = 90$, $\gamma = 120$	0.100
Cc (9)	$a = b = 6.393$, $c = 10.796$, $\alpha = \beta = 88.229$, $\gamma = 146.963$	0.145
$P6_3$mc (186)	$a = b = 3.766$, $c = 16.559$, $\alpha = \beta = 90$, $\gamma = 120$	0.154
R-3c (167)	$a = b = c = 6.794$, $\alpha = \beta = \gamma = 56.359$	0.155

region. Inside the spheres, the basis functions are atomic-like functions written as an expansion in spherical harmonics up to $l_{\max} = 10$. In the interstitial, they are plane waves with a maximum wave vector of magnitude $K_{\max}$. Each plane wave is augmented by one atomic-like function in each muffin-tin sphere. $K_{\max}$ was chosen so that $R_{\mathrm{mt}}K_{\max} = 8$, where R_{mt} is the radius of the smallest muffin-tin sphere in the unit cell. Charge density was Fourier-expanded up to a maximum wave vector of 14 a_0^{-1}, where a_0 is the Bohr radius. Modified Becke-Johnson exchange potential [55], which is known to yield reasonably accurate band gap values in semiconductors, was adopted in our band structure calculations. In the self-consistent field calculations, the total energy and charge were converged to within 0.1 mRy and 0.001 e, respectively. For total energy calculations, a Monkhorst-Pack [67] $8 \times 8 \times 8$ grid of k-points in the Brillouin zone is used.

The phase transition mechanism between stable and metastable structures of $ZnSnS_3$ is characterized using a combination of the variable-cell nudged elastic band method (VCNEB) [68] and the Gibbs construction [69]. VCNEB is an extension of the nudged elastic band (NEB) technique, a widely used method for determining possible reaction paths and saddle points along the minimum energy path (MEP) between endpoints on a potential surface. NEB determines this pathway by using a user defined initial and final structures to generate a set of intermediate structures or "images." These images are then iteratively adjusted in order to minimize the increase in energy along the transition pathway. The traditional NEB algorithm is constrained to maintain a constant unit cell throughout its optimization. VCNEB expands this technique by incorporating lattice parameters into the configuration space, thereby making it suitable for the analysis of phase transition pathways. In particular, it is appropriate for estimating the energy barrier between phases at constant pressure.

Likewise, the Gibbs construction is useful for estimating the pressure at which a specific phase transition will occur. The construction is determined by first plotting the unit cell energy versus volume of a material's stable structures. A tangent line is drawn between the resulting curves. The slope of this line corresponds to the transition pressure between phases of the given material.

We use the VCNEB implementation included with USPEX in combination with VASP to estimate the energy barrier between the stable and metastable phases of $ZnSnS_3$. For the Gibbs construction, we use a combination of VASP and various Python software packages to plot the energies of the scaled $ZnSnS_3$ structures.

3. Results and Discussion

As a rough guide to predicting the stable structure of a compound of the form ABX_3, one usually calculates the Goldschmidt tolerance factor given by

$$t = \frac{r_A + r_X}{\sqrt{2}\,(r_B + r_X)}, \tag{1}$$

where r_A, r_B, and r_X are the radii of the A, B, and X ions, respectively. For Zn, Sn, O, and S, the ionic radii are given, respectively, by 0.74 Å, 0.69 Å, 1.4 Å, and 1.84 Å. Using these values, we find that for $ZnSnO_3$, $t = 0.724$, while for $ZnSnS_3$, $t = 0.721$. One is thus tempted to conclude that the replacement of oxygen with sulfur should not cause a change in structure. However, the large polarizability of sulfur indicates that the Goldschmidt tolerance factor may not be appropriate for predicting the structure of sulfur-containing compounds [70].

To resolve this issue, we carried out extensive calculations using the evolutionary algorithm implemented in USPEX and the PSO method used by CALYPSO. For the USPEX calculation, 20 generations were produced, with each generation containing 40 individuals. With the PSO method, we produced 20 generations, each consisting of 50 individuals. In all cases, the unit cell was assumed to contain two formula units. The most stable structures were identified. To further refine our results, sets of 80 random structures were subsequently generated for each of the most stable space groups. Out of each set, the single structure with the lowest energy was selected, thereby determining the optimal structures and symmetries of $ZnSnS_3$.

In Table 1 we list these $ZnSnS_3$ structures by order of stability. To more easily compare the relative stability of various structures, the free energy per atom in the most stable

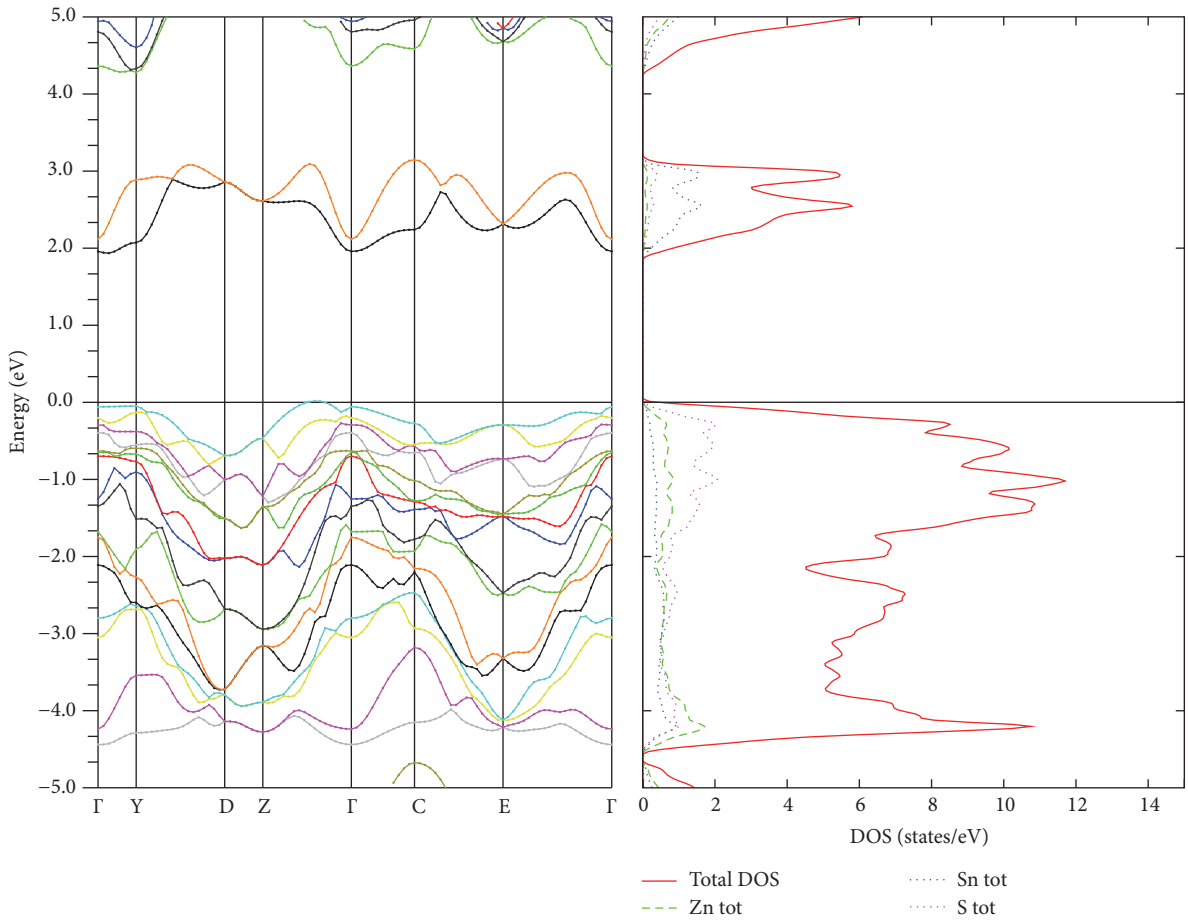

Figure 1: Energy bands in the monoclinic phase (space group number 4) of $ZnSnS_3$, plotted along high symmetry directions, along with a plot of the density of states. The bands are calculated by using the mBJ potential for exchange and correlation. The zero of energy is taken to coincide with the valence band maximum.

structure is set equal to zero. That structure has a monoclinic unit cell with space group $P2_1$ (number 4). The metastable structure with lowest energy is the ilmenite, followed by the LN-type structure. By contrast, in $ZnSnO_3$, the LN-phase is the most stable structure.

To evaluate the usefulness of $ZnSnS_3$ for solar cell applications, we have calculated the band structures of the three most stable phases of this compound. Since low band gap values for light absorbers are essential in photovoltaic applications, it is important that the computational method yield accurate values for these gaps. Density functional theory, when using the local density approximation (LDA) or generalized gradient approximation (GGA) to approximate the exchange-correlation term, severely underestimates band gaps in semiconductors. The use of the modified Becke-Johnson (mBJ) exchange potential results in a significant improvement in calculated band gap values, comparable to that produced by the much more expensive GW approximation. For example, consider the case of $ZnSnO_3$. It has a measured band gap E_g in the range 3.3–3.7 eV [50, 51]. Our calculations, using GGA, give a band gap of 1.5 eV. On the other hand, using the mBJ exchange potential, we calculate a band gap of 3.4 eV, which is in excellent agreement with experiment. We have also calculated the band gaps in $ZnGeO_3$ and $ZnTiO_3$ using the mBJ potential and found them to be 3.57 eV and 3.51 eV, respectively. Though experimental values are not available for the band gaps of these two compounds, the calculated values are typical of those encountered in ferroelectric oxides.

In Figure 1 we present the calculated energy bands and density of states of the monoclinic phase of $ZnSnS_3$ with space group $P2_1$, using the mBJ exchange potential. The band gap is 1.90 eV. Similar calculations on the ilmenite phase of $ZnSnS_3$, with the space group R-3, feature a band gap of 2.30 eV. These two phases of $ZnSnS_3$ are not very useful as light harvesters in solar cells for two reasons: (1) they do not have small band gaps and (2) they are not polar.

The situation is markedly different for the LN-phase of $ZnSnS_3$ with space group R3c (number 161). This phase has a low band gap and a large polarization. In Figure 2 we show the calculated band structure, using the mBJ potential, along with the density of states. Here the band gap is 1.28 eV, in agreement with a previous calculation [53] that used the GW approximation. The upper valence bands are derived mainly from S p-orbitals, while the lower conduction

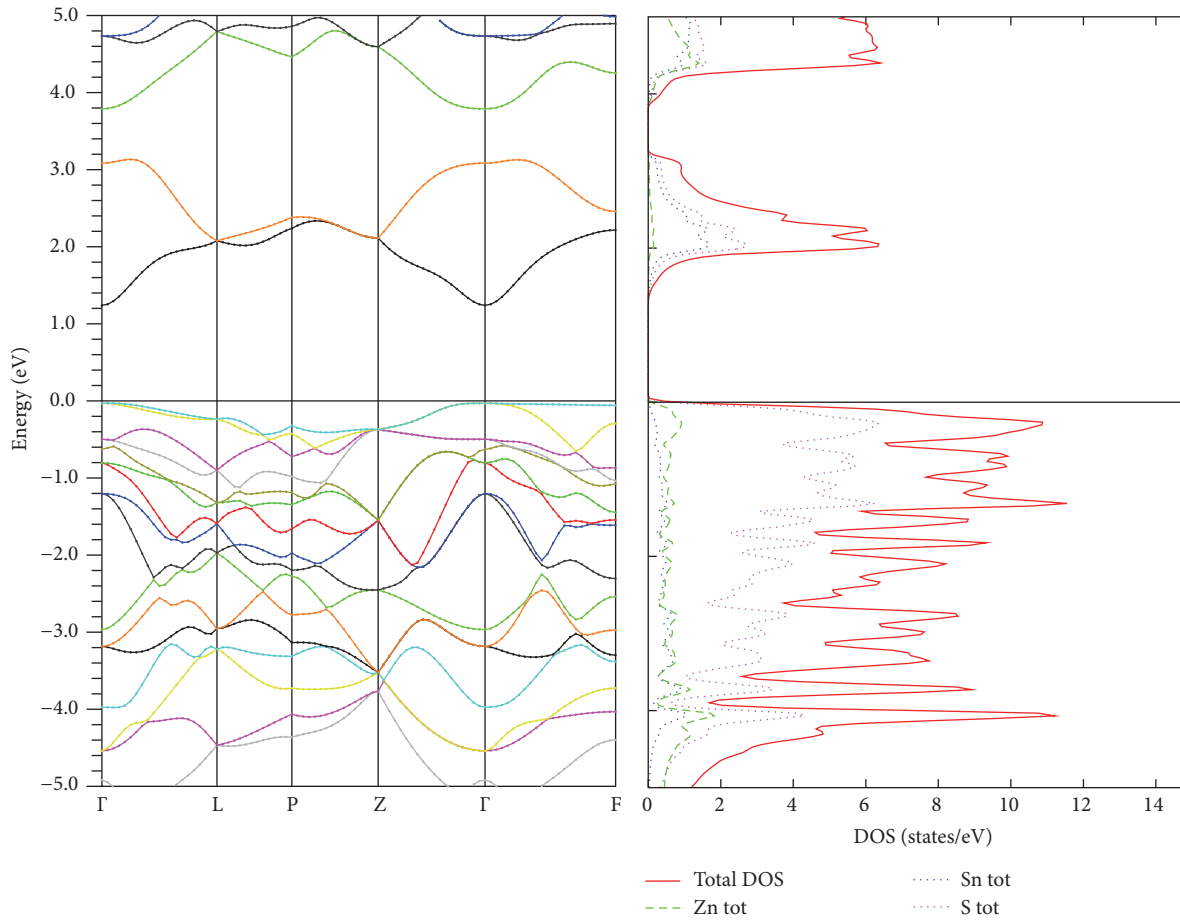

Figure 2: Energy bands in the LN-phase (space group 161) of $ZnSnS_3$, plotted along high symmetry directions, along with a plot of the density of states. The bands are calculated by using the mBJ potential for exchange and correlation. The zero of energy is taken to coincide with the valence band maximum.

bands result mainly from Sn s-orbitals and S p-orbitals. The polarization, calculated using the Berry phase formalism of the modern theory of crystal polarization [71, 72], is found to be 57 $\mu C/cm^2$, which is essentially the same as in the ferroelectric $ZnSnO_3$. About one-third of the polarization is electronic; the rest is ionic. The large ionic polarization derives from the particular crystal structure of this phase of $ZnSnS_3$. Though the Sn ion is octahedrally bonded to six S ions, it does not sit at the center of the octahedron; rather, three of the six Sn-S bonds have a length of 2.42 Å while the other three have a length of 2.57 Å. Hybridization between the Sn s-orbitals and S p-orbitals causes a displacement of the Sn ion from the center of the octahedron, thereby lowering the energy of the system.

As indicated earlier, the monoclinic structure is the most stable phase of $ZnSnS_3$, while the LN-phase is metastable. We now consider the possible transition between these two phases. A variable-cell nudged elastic band (VCNEB) calculation is carried out in order to map out the transition path connecting the two phases. The minimum energy path between the monoclinic and LN-type structures is shown in Figure 3. From the figure we see that an energy barrier of 4.52 eV (0.452 eV/atom) separates the phases. The lattice parameters of the path's terminal structures and two intermediate metastable structures are presented in Table 2. The high energy barrier present at zero temperature and pressure suggests that, while not the lowest energy configuration of $ZnSnS_3$, it is highly unlikely that the LN-phase, once established, would revert to the monoclinic phase at room temperature.

Table 2: Evolution of $ZnSnS_3$ cell structure transition pathway.

Lattice constants (Å)	Lattice angles α, β, γ (degrees)	Space group
10.4900, 3.7518, 6.3083	89.999, 55.314, 89.999	$P2_1$ (4)
8.4274, 5.3596, 6.8366	71.523, 50.845, 68.122	P1 (1)
8.6655, 5.6717, 6.9900	64.035, 49.581, 64.901	P1 (1)
6.7211, 6.7211, 6.7211	55.756, 55.756, 55.756	R3c (161)

By using the Gibbs construction, discussed earlier in Section 2, we can make a rough estimate of the pressure which, at zero temperature, will induce a structural phase transition in $ZnSnS_3$ from the monoclinic phase to the LN-phase. This is illustrated in Figure 4, which indicates that the phase transition takes place at a pressure of 16 GPa.

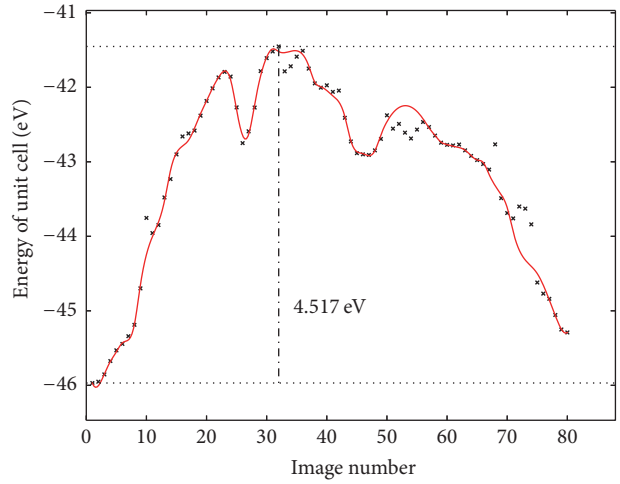

Figure 3: Progression of unit cell energies of structures forming a transition pathway between states of $ZnSnS_3$. Path begins with a stable structure exhibiting space group 4 symmetry and ends with one having space group 161 symmetry. The initial and maximum energies are used to estimate the energy barrier to transition.

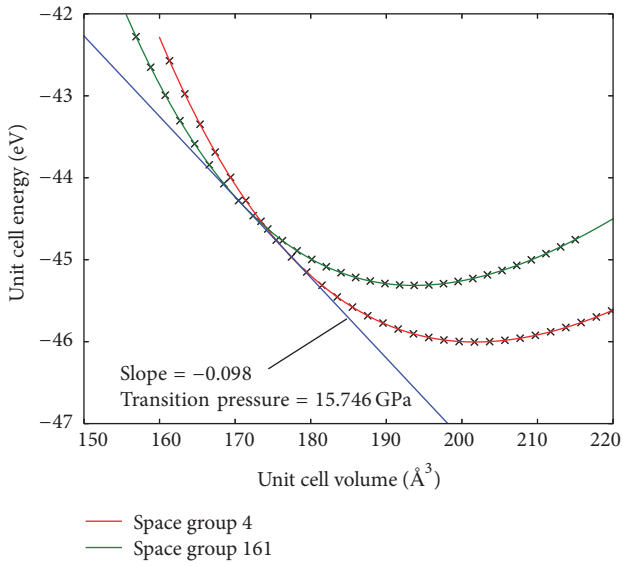

Figure 4: Calculation of transition pressure using the Gibbs construction. Stable space group 4 and space group 161 structures are volumetrically scaled, with their energies calculated using VASP. The slope of the tangent line between the two resulting curves corresponds to the transition pressure between states.

Finally, we examine the formation and stability of $ZnSnS_3$ by comparing its free energy to that of some potential precursors at zero temperature. We note that $ZnSnO_3$ is formed by a solid-state reaction of ZnO and SnO_2 at high temperature and pressure. At zero temperature and zero pressure, our calculations indicate that the free energies of ZnO, SnO_2, and $ZnSnO_3$ are, respectively, −5.29 eV/atom, −7.09 eV/atom, and −6.35 eV/atom. The average free energy per atom of $ZnSnO_3$ is thus higher than that of a mixture of ZnO and SnO_2 by 0.02 eV. However, at zero temperature and a pressure of 7 GPa, the per-atom energy of $ZnSnO_3$ drops below that of its precursor mixture by 0.005 eV. This helps explain how it is possible to form stable $ZnSnO_3$ from compounds with apparently higher stability. Furthermore, when $ZnSnO_3$ is returned to ambient conditions, it remains stable, rather than decomposing into smaller, lower-energy compounds.

We apply the same reasoning to $ZnSnS_3$, assuming that it may be formed at high temperature by applying pressure to a mixture of ZnS and SnS_2. At zero temperature and pressure, the free energies of ZnS and SnS_2 are −4.10 eV/atom and −5.00 eV/atom, respectively, yielding a combined per-atom energy of −4.64 eV. For $ZnSnS_3$, on the other hand, the calculated energy is −4.60 eV/atom, which is higher than that of its precursors by 0.04 eV/atom. However, at zero temperature and a pressure of 18 GPa, our calculations indicate that the free energy per atom of $ZnSnS_3$ is lower than the combined per-atom free energy of ZnS and SnS_2 by 0.004 eV. This indicates that it is possible for $ZnSnS_3$ to form, albeit at relatively high pressure. Importantly, these energies were calculated at zero temperature and, in practice, the addition of heat energy may further lower the pressure at which $ZnSnS_3$ forms. The analogous example of $ZnSnO_3$, along with the high energy barriers between phases of $ZnSnS_3$, leads us to believe that, once formed, $ZnSnS_3$ would be stable at ambient conditions.

4. Conclusions

As anticipated, our calculations indicate that the substitution of sulfur for oxygen in $ZnSnO_3$ reduces its band gap, particularly for the LN-phase. This reduction is sufficient to bring the absorption band of $ZnSnS_3$ into the visible to mid-infrared spectrum, thereby making it suitable for solar cell applications. An unexpected result of the substitution is that a monoclinic phase becomes the most stable structure of $ZnSnS_3$. It is likely that a suitable application of temperature and pressure may transition $ZnSnS_3$ to its LN-phase. VCNEB calculations for $ZnSnS_3$ suggest that it will not revert from its LN-phase (once attained) to its monoclinic phase at room temperature. Furthermore, the Gibbs construction specifies the transition pressure between phases to be roughly 16 GPa, a pressure that is not difficult to attain in the lab but is sufficiently high to allow for a persistent metastable structure under typical atmospheric conditions.

Further work is needed to characterize the precise conditions under which transition to the polar LN-phase occurs. The application of transition path sampling (TPS) to further evaluate the transition path produced by VCNEB may help to better identify the most likely pathway between stable and metastable states in $ZnSnS_3$. Finally, the effect of oxygen to sulfur substitution in other oxides such as $ZnGeO_3$ and $ZnTiO_3$ should be evaluated.

Competing Interests

The authors report no conflict of interests in this research.

Acknowledgments

The authors gratefully acknowledge support by the National Science Foundation under Grant no. HRD-1547723 and the NSF PREM Program: Cal State LA & Penn State Partnership for Materials Research and Education, Award DMR-1523588. The authors also acknowledge partial support by the Materials Simulation Center and the Material Research Institute at Penn-State University.

References

[1] D. Cao, C. Wang, F. Zheng, W. Dong, L. Fang, and M. Shen, "High-efficiency ferroelectric-film solar cells with an n-type Cu_2O cathode buffer layer," *Nano Letters*, vol. 12, no. 6, pp. 2803–2809, 2012.

[2] M. Alexe and D. Hesse, "Tip-enhanced photovoltaic effects in bismuth ferrite," *Nature Communications*, vol. 2, no. 1, article 256, 2011.

[3] M. Qin, K. Yao, and Y. C. Liang, "High efficient photovoltaics in nanoscaled ferroelectric thin films," *Applied Physics Letters*, vol. 93, no. 12, Article ID 122904, 2008.

[4] T. Choi, S. Lee, Y. J. Choi, V. Kiryukhin, and S.-W. Cheong, "Switchable ferroelectric diode and photovoltaic effect in $BiFeO_3$," *Science*, vol. 324, no. 5923, pp. 63–66, 2009.

[5] K. T. Butler, J. M. Frost, and A. Walsh, "Ferroelectric materials for solar energy conversion: photoferroics revisited," *Energy & Environmental Science*, vol. 8, no. 3, pp. 838–848, 2015.

[6] Y. Yuan, Z. Xiao, B. Yang, and J. Huang, "Arising applications of ferroelectric materials in photovoltaic devices," *Journal of Materials Chemistry A*, vol. 2, no. 17, pp. 6027–6041, 2014.

[7] S. Y. Yang, J. Seidel, S. J. Byrnes et al., "Above-bandgap voltages from ferroelectric photovoltaic devices," *Nature Nanotechnology*, vol. 5, no. 2, pp. 143–147, 2010.

[8] Y. Inoue, K. Sato, K. Sato, and H. Miyama, "Photoassisted water decomposition by ferroelectric lead zirconate titanate ceramics with anomalous photovoltaic effects," *Journal of Physical Chemistry*, vol. 90, no. 13, pp. 2809–2810, 1986.

[9] S. M. Young and A. M. Rappe, "First-principles calculation of the shift current photovoltaic effect in ferroelectrics," *Physical Review Letters*, vol. 109, no. 11, Article ID 116601, 2012.

[10] H. Huang, "Solar energy: ferroelectric photovoltaics," *Nature Photonics*, vol. 4, no. 3, pp. 134–135, 2010.

[11] Y. Yuan, T. J. Reece, P. Sharma et al., "Efficiency enhancement in organic solar cells with ferroelectric polymers," *Nature Materials*, vol. 10, no. 4, pp. 296–302, 2011.

[12] J. W. Bennett, L. Grinberg, and A. M. Rappe, "New highly polar semiconductor ferroelectrics through d^8 cation-O vacancy substitution into $PbTi0_3$: a theoretical study," *Journal of the American Chemical Society*, vol. 130, no. 51, pp. 17409–17412, 2008.

[13] V. M. Fridkin and B. Popov, "Anomalous photovoltaic effect in ferroelectrics," *Soviet Physics Uspekhi*, vol. 21, no. 12, pp. 981–991, 1978.

[14] V. M. Fridkin, *Photoferroelectrics*, Springer, Berlin, Germany, 1979.

[15] A. M. Glass, D. Von Der Linde, and T. J. Negran, "High−voltage bulk photovoltaic effect and the photorefractive process in $LiNbO_3$," *Applied Physics Letters*, vol. 25, no. 4, pp. 233–235, 1974.

[16] A. G. Chynoweth, "Surface space-charge layers in barium titanate," *Physical Review*, vol. 102, no. 3, pp. 705–714, 1956.

[17] G. F. Neumark, "Theory of the anomalous photovoltaic effect of ZnS," *Physical Review*, vol. 125, no. 3, pp. 838–845, 1962.

[18] W. S. Choi, M. F. Chisholm, D. J. Singh, T. Choi, G. E. Jellison Jr., and H. N. Lee, "Wide band gap tunability in complex transition metal oxides by site-specific substitution," *Nature Communications*, vol. 3, article 689, 2012.

[19] S. Ehara, K. Muramatsu, M. Shimazu et al., "Dielectric properties of $Bi_4Ti_3O_{12}$ below the curie temperature," *Japanese Journal of Applied Physics*, vol. 20, no. 5, pp. 877–881, 1981.

[20] D. J. Singh, S. S. A. Seo, and H. N. Lee, "Optical properties of ferroelectric $Bi_4\ Ti_3\ O_{12}$," *Physical Review B—Condensed Matter and Materials Physics*, vol. 82, no. 18, Article ID 180103, 2010.

[21] C. Jia, Y. Chen, and W. F. Zhang, "Optical properties of aluminum-, gallium-, and indium-doped $Bi_4Ti_3O_{12}$ thin films," *Journal of Applied Physics*, vol. 105, no. 11, Article ID 113108, 2009.

[22] T. Arima, Y. Tokura, and J. B. Torrance, "Variation of optical gaps in perovskite-type 3d transition-metal oxides," *Physical Review B*, vol. 48, no. 23, pp. 17006–17009, 1993.

[23] I. Grinberg, D. V. West, M. Torres et al., "Perovskite oxides for visible-light-absorbing ferroelectric and photovoltaic materials," *Nature*, vol. 503, no. 7477, pp. 509–512, 2013.

[24] S. R. Basu, "Photoconductivity in $BiFeO_3$ thin films," *Applied Physics Letters*, vol. 92, no. 9, Article ID 091905, 2008.

[25] A. J. Hauser, J. Zhang, L. Mier et al., "Characterization of electronic structure and defect states of thin epitaxial $BiFeO_3$ films by UV-visible absorption and cathodoluminescence spectroscopies," *Applied Physics Letters*, vol. 92, no. 22, Article ID 222901, 2008.

[26] R. Nechache, C. Harnagea, A. Pignolet et al., "Growth, structure, and properties of epitaxial thin films of first-principles predicted multiferroic Bi_2FeCrO_6," *Applied Physics Letters*, vol. 89, no. 10, Article ID 102902, 2006.

[27] R. Nechache, C. Harnagea, L.-P. Carignan, D. Ménard, and A. Pignolet, "Epitaxial Bi_2FeCrO_6 multiferroic thin films," *Philosophical Magazine Letters*, vol. 87, no. 3-4, pp. 231–240, 2007.

[28] R. Nechache, C. Harnagea, S. Li et al., "Bandgap tuning of multiferroic oxide solar cells," *Nature Photonics*, vol. 9, no. 1, pp. 61–67, 2014.

[29] Y. Inaguma, M. Yoshida, and T. Katsumata, "A polar oxide $ZnSnO_3$ with a $LiNbO_3$-type structure," *Journal of the American Chemical Society*, vol. 130, no. 21, pp. 6704–6705, 2008.

[30] Y. Inaguma, M. Yoshida, T. Tsuchiya et al., "High-pressure synthesis of novel lithium niobate-type oxides," *Journal of Physics: Conference Series*, vol. 215, no. 1, Article ID 012131, 2010.

[31] Y. Inaguma, K. Tanaka, T. Tsuchiya et al., "Synthesis, structural transformation, thermal stability, valence state, and magnetic and electronic properties of $PbNiO_3$ with perovskite- and $LiNbO_3$-type structures," *Journal of the American Chemical Society*, vol. 133, no. 42, pp. 16920–16929, 2011.

[32] R. Arielly, W. M. Xu, E. Greenberg et al., "Intriguing sequence of $GaFeO_3$ structures and electronic states to 70 GPa," *Physical Review B*, vol. 84, no. 9, Article ID 094109, 2011.

[33] Y. Shi, Y. Guo, X. Wang et al., "A ferroelectric-like structural transition in a metal," *Nature Materials*, vol. 12, no. 11, pp. 1024–1027, 2013.

[34] H. Yusa, M. Akaogi, N. Sata, H. Kojitani, R. Yamamoto, and Y. Ohishi, "High-pressure transformations of ilmenite to perovskite, and lithium niobate to perovskite in zinc germanate,"

Physics and Chemistry of Minerals, vol. 33, no. 3, pp. 217–226, 2006.

[35] M. Akaogi, H. Kojitani, H. Yusa, R. Yamamoto, M. Kido, and K. Koyama, "High-pressure transitions and thermochemistry of $MGeO_3$ (M=Mg, Zn and Sr) and Sr-silicates: systematics in enthalpies of formation of $A^{2+}B^{4+}O_3$ perovskites," *Physics and Chemistry of Minerals*, vol. 32, no. 8-9, pp. 603–613, 2005.

[36] J. Zhang, B. Xu, Z. Qin, X. F. Li, and K. L. Yao, "Ferroelectric and nonlinear optical properties of the $LiNbO_3$-type $ZnGeO_3$ from first-principles study," *Journal of Alloys and Compounds*, vol. 514, pp. 113–119, 2012.

[37] Y. Inaguma, A. Aimi, Y. Shirako et al., "High-pressure synthesis, crystal structure, and phase stability relations of a $LiNbO_3$-type polar titanate $ZnTiO_3$ and its reinforced polarity by the second-order Jahn-Teller effect," *Journal of the American Chemical Society*, vol. 136, no. 7, pp. 2748–2756, 2014.

[38] Y. Syono, S.-I. Akimoto, Y. Ishikawa, and Y. Endoh, "A new high pressure phase of $MnTiO_3$ and its magnetic property," *Journal of Physics and Chemistry of Solids*, vol. 30, no. 7, pp. 1665–1672, 1969.

[39] E. Ito and Y. Matsui, "High-pressure transformations in silicates, germanates, and titanates with ABO_3 stoichiometry," *Physics and Chemistry of Minerals*, vol. 4, no. 3, pp. 265–273, 1979.

[40] J. Ko and C. T. Prewitt, "High-pressure phase transition in $MnTiO_3$ from the ilmenite to the $LiNbO_3$ structure," *Physics and Chemistry of Minerals*, vol. 15, no. 4, pp. 355–362, 1988.

[41] N. L. Ross, J. Ko, and C. T. Prewitt, "A new phase transition in $MnTiO_3$: $LiNbO_3$-perovskite structure," *Physics and Chemistry of Minerals*, vol. 16, no. 7, pp. 621–629, 1989.

[42] Y. Syono, H. Sawamoto, and S. Akimoto, "Disordered ilmenite $MnSnO_3$ and its magnetic property," *Solid State Communications*, vol. 7, no. 9, pp. 713–716, 1969.

[43] K. Leinenweber, W. Utsumi, Y. Tsuchida, T. Yagi, and K. Kurita, "Unquenchable high-pressure perovskite polymorphs of $MnSnO_3$ and $FeTiO_3$," *Physics and Chemistry of Minerals*, vol. 18, no. 4, pp. 244–250, 1991.

[44] A. Mehta, K. Leinenweber, A. Navrotsky, and M. Akaogi, "Calorimetric study of high pressure polymorphism in $FeTiO_3$: stability of the perovskite phase," *Physics and Chemistry of Minerals*, vol. 21, no. 4, pp. 207–212, 1994.

[45] K. Leinenweber, J. Linton, A. Navrotsky, Y. Fei, and J. B. Parise, "High-pressure perovskites on the join $CaTiO_3$-$FeTiO_3$," *Physics and Chemistry of Minerals*, vol. 22, no. 4, pp. 251–258, 1995.

[46] T. Hattori, T. Matsuda, T. Tsuchiya, T. Nagai, and T. Yamanaka, "Clinopyroxene-perovskite phase transition of $FeGeO_3$ under high pressure and room temperature," *Physics and Chemistry of Minerals*, vol. 26, no. 3, pp. 212–216, 1999.

[47] K. Leinenweber, Y. Wang, T. Yagi, and H. Yusa, "An unquenchable perovskite phase of $MgGeO_3$ and comparison with $MgSiO_3$ perovskite," *American Mineralogist*, vol. 79, no. 1-2, pp. 197–199, 1994.

[48] A. W. Sleight and C. T. Prewitt, "Preparation of $CuNbO_3$ and $CuTaO_3$ at high pressure," *Materials Research Bulletin*, vol. 5, no. 3, pp. 207–211, 1970.

[49] M. Akaogi, K. Abe, H. Yusa, H. Kojitani, D. Mori, and Y. Inaguma, "High-pressure phase behaviors of $ZnTiO_3$: ilmenite-perovskite transition, decomposition of perovskite into constituent oxides, and perovskite-lithium niobate transition," *Physics and Chemistry of Minerals*, vol. 42, no. 6, pp. 421–429, 2015.

[50] A. V. Borhade and Y. R. Baste, "Study of photocatalytic asset of the $ZnSnO_3$ synthesized by green chemistry," *Arabian Journal of Chemistry*, 2012.

[51] H. Mizoguchi and P. M. Woodward, "Electronic structure studies of main group oxides possessing edge-sharing octahedra: implications for the design of transparent conducting oxides," *Chemistry of Materials*, vol. 16, no. 25, pp. 5233–5248, 2004.

[52] B. Kolb and A. Kolpak, "Zinc stannate as a solar cell material," *Bulletin of the American Physical Society*, vol. 59, 2014.

[53] B. Kolb and A. M. Kolpak, "First-principles design and analysis of an efficient, Pb-free ferroelectric photovoltaic absorber derived from $ZnSnO_3$," *Chemistry of Materials*, vol. 27, no. 17, pp. 5899–5906, 2015.

[54] C. Kons, A. Datta, and P. Mukherjee, "Band-gap tuning in perovskite-type ferroelectric $ZnSnO_3$ by doping and core shell approach for solar cell applications," *Bulletin of the American Physical Society*, vol. 60, no. 1, 2015.

[55] F. Tran and P. Blaha, "Accurate band gaps of semiconductors and insulators with a semilocal exchange-correlation potential," *Physical Review Letters*, vol. 102, no. 22, Article ID 226401, 2009.

[56] T. Kosugi, K. Murakami, and S. Kaneko, *Thin-Film Structures for Photovoltaics*, Materials Research Society, Symposium, 1997.

[57] N. Barreau, J. C. Bernède, S. Marsillac, and A. Mokrani, "Study of low temperature elaborated tailored optical band gap β-$In_2S_{3-3x}O_{3x}$ thin films," *Journal of Crystal Growth*, vol. 235, no. 1–4, pp. 439–449, 2002.

[58] K. Ogisu, A. Ishikawa, Y. Shimodaira, T. Takata, H. Kobayashi, and K. Domen, "Electronic band structures and photochemical properties of La-Ga-based oxysulfideslfides," *Journal of Physical Chemistry C*, vol. 112, no. 31, pp. 11978–11984, 2008.

[59] A. R. Oganov and C. W. Glass, "Crystal structure prediction using *ab* initio evolutionary techniques: Principles and applications," *The Journal of Chemical Physics*, vol. 124, no. 24, Article ID 244704, 2006.

[60] A. O. Lyakhov, A. R. Oganov, H. T. Stokes, and Q. Zhu, "New developments in evolutionary structure prediction algorithm USPEX," *Computer Physics Communications*, vol. 184, no. 4, pp. 1172–1182, 2013.

[61] A. R. Oganov, A. O. Lyakhov, and M. Valle, "How evolutionary crystal structure prediction works-and why," *Accounts of Chemical Research*, vol. 44, no. 3, pp. 227–237, 2011.

[62] Y. Wang, J. Lv, L. Zhu, and Y. Ma, "CALYPSO: a method for crystal structure prediction," *Computer Physics Communications*, vol. 183, no. 10, pp. 2063–2070, 2012.

[63] G. Kresse and J. Hafner, "*Ab initio* molecular dynamics for liquid metals," *Physical Review B*, vol. 47, no. 1, pp. 558–561, 1993.

[64] G. Kresse and J. Furthmüller, "Efficiency of ab-initio total energy calculations for metals and semiconductors using a plane-wave basis set," *Computational Materials Science*, vol. 6, no. 1, pp. 15–50, 1996.

[65] G. Kresse and D. Joubert, "From ultrasoft pseudopotentials to the projector augmented-wave method," *Physical Review B*, vol. 59, no. 3, pp. 1758–1775, 1999.

[66] P. Blaha, K. Schwarz, G. Madsen, D. Kvasnicka, and J. Luitz, "User's Guide: WIEN2K: an augmented plane wave + local orbitals program for calculating crystal properties," 2001.

[67] H. J. Monkhorst and J. D. Pack, "Special points for Brillouin-zone integrations," *Physical Review. B. Solid State*, vol. 13, no. 12, pp. 5188–5192, 1976.

[68] G.-R. Qian, X. Dong, X.-F. Zhou, Y. Tian, A. R. Oganov, and H.-T. Wang, "Variable cell nudged elastic band method for studying solid-solid structural phase transitions," *Computer Physics Communications*, vol. 184, no. 9, pp. 2111–2118, 2013.

[69] M. T. Yin and M. L. Cohen, "Theory of static structural properties, crystal stability, and phase transformations: application to Si and Ge," *Physical Review B*, vol. 26, no. 10, pp. 5668–5687, 1982.

[70] J. A. Brehm, J. W. Bennett, M. R. Schoenberg, I. Grinberg, and A. M. Rappe, "The structural diversity of ABS_3 compounds with d^0 electronic configuration for the *B*-cation," *The Journal of Chemical Physics*, vol. 140, no. 22, Article ID 224703, 2014.

[71] R. Resta, "Macroscopic electric polarization as a geometric quantum phase," *Europhysics Letters*, vol. 22, no. 2, pp. 133–138, 1993.

[72] R. D. King-Smith and D. Vanderbilt, "Theory of polarization of crystalline solids," *Physical Review B*, vol. 47, no. 3, pp. 1651–1654, 1993.